Published online 10 January 2012 *Nucleic Acids Research, 2012, Vol. 40, No. 9* ***3913–3928***
doi:10.1093/nar/gkr1300

The molecular basis of ATM-dependent dimerization of the Mdc1 DNA damage checkpoint mediator

Stephanie Jungmichel[1,5], Julie A. Clapperton[2], Janette Lloyd[2], Flurina J. Hari[1], Christoph Spycher[1], Lucijana Pavic[1], Jiejin Li[2], Lesley F. Haire[2], Mario Bonalli[1], Dorthe H. Larsen[1], Claudia Lukas[3], Jiri Lukas[3], Derek MacMillan[4], Michael L. Nielsen[5], Manuel Stucki[1,*] and Stephen J. Smerdon[2,*]

[1]Institute of Veterinary Biochemistry and Molecular Biology, University of Zürich – Irchel, Winterthurerstrasse 190, CH-8057 Zürich, Switzerland, [2]MRC National Institute of Medical Research, Division of Protein Structure, The Ridgeway, Mill Hill, London NW7 1AA, UK, [3]Institute of Cancer Biology and Centre for Genotoxic Stress Research, Danish Cancer Society, Strandboulevarden 49, DK-2100, Copenhagen, Denmark, [4]Department of Chemistry, University College, London WC1H 0AJ, UK and [5]Department of Proteomics, The Novo-Nordisk Foundation Center for Protein Research, University of Copenhagen, Faculty of Health Sciences, Biegdamsvej 3B DK-2200, Copenhagen, Denmark

Received October 14, 2011; Revised December 16, 2011; Accepted December 18, 2011

ABSTRACT

Mdc1 is a large modular phosphoprotein scaffold that maintains signaling and repair complexes at double-stranded DNA break sites. Mdc1 is anchored to damaged chromatin through interaction of its C-terminal BRCT-repeat domain with the tail of γH2AX following DNA damage, but the role of the N-terminal forkhead-associated (FHA) domain remains unclear. We show that a major binding target of the Mdc1 FHA domain is a previously unidentified DNA damage and ATM-dependent phosphorylation site near the N-terminus of Mdc1 itself. Binding to this motif stabilizes a weak self-association of the FHA domain to form a tight dimer. X-ray structures of free and complexed Mdc1 FHA domain reveal a 'head-to-tail' dimerization mechanism that is closely related to that seen in pre-activated forms of the Chk2 DNA damage kinase, and which both positively and negatively influences Mdc1 FHA domain-mediated interactions in human cells prior to and following DNA damage.

INTRODUCTION

Genomic integrity is constantly challenged by the effects of DNA-damaging agents. Double-stranded DNA breaks (DSBs) are considered to be the most genotoxic lesions since incorrect repair can lead to chromosome breaks and other aberrations that are characteristic of and which may lead to cancer. DSBs initiate a program of cellular responses involving activation of cell-cycle checkpoints and deployment of the repair machinery. Central to DNA damage response (DDR) regulation is a protein kinase cascade involving ataxia telangiectasia-mutated kinase (ATM), which acts as sensor of DSBs, initiating damage signals that are propagated through phosphorylation of checkpoint kinases and other diverse downstream targets (1). Many of these phosphorylation events are now known to initiate protein–protein interactions mediated by phosphoserine/threonine-specific binding domains, most commonly forkhead-associated (FHA) and Brca1 C-terminal (BRCT) modules (2), providing for highly regulated, physical links between DDR components.

Mediator of the DNA damage Checkpoint-1 (Mdc1) is a modular, 2089 amino acid protein originally identified as an essential factor for establishment of DNA damage checkpoints (3–6). It functions as an assembly platform for the localization and maintenance of signaling and repair factors at and around DSB sites (7). As such, Mdc1 is a founding member of a class of large scaffolding/adaptor proteins known as 'mediators' that includes proteins such as human Brca1, 53BP1 and yeast Rad9 and Crb2. While all of these molecules contain two or more

*To whom correspondence should be addressed. Tel: +44 208 816 2533; Fax: +44 208 816 2580; Email: stephen.smerdon@nimr.mrc.ac.uk
Correspondence may also be addressed to Manuel Stucki. Email: Manuel.Stucki@usz.ch
Present address:
Manuel Stucki, Department of Gynecology, University Hospital Zurich, Wagistrasse 14, CH-8952 Schlieren, Switzerland.

The authors wish it to be known that, in their opinion, the first two authors should be regarded as joint First Authors.

copies of BRCT-repeat motifs, Mdc1 uniquely contains an additional FHA domain at its N-terminus.

Functionally, the C-terminal BRCT-repeats tether Mdc1 to regions of DNA damage by virtue of their specific binding to ATM-phosphorylated H2AX (known as γH2AX), a variant histone H2A, which acts as the primary marker of damaged chromatin in all eukaryotic cells (8). In contrast, the function of the FHA domain is less clear but has been suggested to include interaction with ATM itself (9,10), Chk2 (3), components of the Mre11/Rad50/Nbs1 (MRN) complex (5,11) and other repair proteins such as Rad51 (12). We now show that the Mdc1 FHA domain mediates an inter-molecular interaction with a previously uncharacterized ATM phosphorylation site located within its own N-terminal region, revealing a role for DNA damage-inducible Mdc1 dimerization in the cellular response to double-stranded DNA breaks with a more general significance for understanding regulatory mechanisms that underpin FHA domain function in other signaling contexts.

MATERIALS AND METHODS

Plasmids

Human Mdc1-GST constructs were previously described (13) Human Mdc1 (800) comprising amino acids 1–800 was generated by PCR and C-terminally tagged with HA/FLAG and Myc, respectively, and cloned into pcDNA3.1 (+) mammalian expression vector (Invitrogen). The Mdc1 FHA domain-containing fragment (amino acids 1–154) was amplified by PCR and cloned into a modified pEYFP-nuc vector (Clontech), in which two tetracycline-repressor binding elements were inserted between promotor and coding sequences to generate an inducible expression cassette (8). Point mutations were introduced by PCR-based methods or using the QuikChange Site-Directed Mutagenesis kit (Stratagene).

Protein expression and purification

DNA fragments encoding human Mdc1 residues 1–138, 19–138 or 27–138 were amplified from a Mdc1 cDNA clone and ligated into BamH1/Xho1 digested pGEX-6P1. GST-fusion proteins were affinity purified on glutathione-4B resin (Amersham) and cleaved from the affinity resin with rhinovirus 3C protease overnight at 4°C. Cleaved Mdc1 fragments were further purified by gel-filtration chromatography on Superdex 75.

Structure solution and refinement

The structure of the selenomethionine peptide complex was solved by the single-wavelength anomalous diffraction (SAD) method using data collected on beamline 10.1 at the SRS Daresbury, UK. Four selenium sites were located and phases refined by SOLVE/RESOLVE (14). The resulting map was readily interpretable allowing an essentially complete model for the two complexes in the asymmetric unit. The resulting FHA domain structure was then used to solve the non-complexed crystal form by molecular replacement using PHASER (15). Model-building was carried out with 'Coot' (16) and both structures were refined using REFMAC5 (17).

Cell culture and gene transfer

$Mdc1^{-/-}$ and $Mdc1^{+/+}$ MEFs were gifts from J. Chen (University of Texas MD Anderson Cancer Center, Houston, TX, USA). U2OS, HEK 293T and MEFs were grown in D-MEM (Invitrogen) supplemented with 10% FCS (Gibco) and streptomycin/penicillin (100 U/ml, Gibco). Transfection of plasmids was done using either FuGene 6 (Roche) or calcium phosphate. U2OS-TetOn cells stably expressing the tetracycline repressor were generated by transfection of EYFP-tagged Mdc1-FHA domain following selection in G418-containing medium (Calbiochem). The siRNA oligonucleotides against endogenous human Mdc1 were purchased from Ambion (siRNA ID: 21738) containing the following sequence: sense 5′-GGAUCACACAAAGAUUAGAtt and antisense 5′-UCUAAUCUUUGUGUGAUCCtt. SiRNA transfections were performed using Lipofectamine RNAiMAX (Invitrogen) according the manufacturer's protocol. DNA damage was induced in a Faxitron X-ray cabinet at 5–10 Gy/min. or by means of single-cell laser microirradiation (see below).

Antibodies

The mouse monoclonal γH2AX antibody was obtained from Millipore and the rabbit polyclonal c-Myc antibody (sc-789) from Santa Cruz Biotechnology. The rabbit polyclonal FLAG antibody and the anti-FLAG M2 affinity gel, used for co-immunoprecipitation, were purchased from Sigma. Rabbit polyclonal Mdc1(889) and sheep polyclonal Mdc1(3835) antibodies were raised against Mdc1-FHA-GST as described previously (5). The phosphospecific antibody Mdc1 'pT4' was raised in rabbit against the phosphopeptide MED(pT)QAIDWDVC and affinity purified using the phosphorylated and non-phosphorylated peptide (Eurogentec). Rabbit polyclonal ATM antiserum for ATM immunoprecipitation was a kind gift from Graeme Smith (KuDOS Pharmaceuticals, Cambridge, UK).

Expressed protein ligation

Purified Mdc1 1–158 was digested with trypsin (Promega) at a ratio of 1:250 w/w enzyme:substrate to yield a 112 residue fragment (26–138) containing the FHA domain and part of the preceding linker with Cys-26 at its N-terminus. Synthesis of a C-terminally protected pThr-4 peptide (MEDpTQAIDWDVEEEEETEQSSESL R-SBn) and *in vitro* ligation to the Mdc1 26–138 fragments were carried in 200 mM phosphate buffer pH 8.0, 150 mM NaCl, 10 mM TCEP, 2% w/v 2-mercaptoethanesulphonic acid overnight at room temperature.

Pulldown of Mdc1–FHA interaction partners

Stable, Doxocycline-inducible cell lines were generated by co-transfecting U2OS cells with pcDNA6/TO expressing the Tet-repressor and pcDNA5/TO expressing a

C-terminally Strep-tagged Mdc1-FHA domain (amino acids 1–154). Stable clones were selected with Hygromycin B (Sigma) and Blasticidin (Invitrogen) and subsequently cultured in DMEM supplemented with 10% dialyzed FBS (Invitrogen) and either L-lysine (Lys0) and L-arginine (Arg0), L-lysine 4,4,5,5-D4 (Lys4) and L-arginine–U-$^{13}C_6$ (Arg6) or L-lysine–U-$^{13}C_6$-$^{15}N_2$ (Lys8) and L-arginine–U-$^{13}C_6$-$^{15}N_4$ (Arg10) (Cambridge Isotope Laboratory) as described previously (18). Following 16 h of doxocyclin induction and IR treatment (10 Gy for 30 min), cells were lysed in buffer containing 50 mM Tris–HCl (pH 7.5), 150 mM NaCl, 1 mM EDTA, 1 mM $MgCl_2$,1% NP-40, 2 mM Na-orthovanadate, 5 mM NaF, 5 mM glycero-2-phosphate and protease inhibitors (Complete^{TM} tablets, Roche). Equal protein amounts were incubated with Strep-Tactin Sepharose (IBA BioTAGnology) and bound complexes were eluated in Laemmli sample buffer, combined and resolved on 4–20% SDS–PAGE. The CB-stained gel was cut into slices, proteins were digested with trypsin and loaded on to C18 stage tips prior to mass spectrometric analysis.

Mass spectrometric analysis

MS analysis was performed on a nanoscale HPLC system (Easy-nLC from Proxeon) connected to a hybrid LTQ Orbitrap Velos mass spectrometer (Thermo Scientific). Peptides were separated over a 110 min linear gradient from 5% to 40% acetonitrile in 0.5% acetic acid with a flow rate of 250 nl/min. Survey full scan MS spectra were acquired from m/z 300 to 1700 in the Orbitrap detector with a resolution of $R = 30\,000$ followed by isolation and fragmentation of the 10 most intense ions using HCD (higher energy collisional activation dissociation) at resolution $R = 7500$ (19). Raw data files were processed with the MaxQuant software suite (www.maxquant.org). Proteins and peptides were identified by Mascot database search against a target/decoy (forward and reversed) version of the IPI human database 3.80 with a false discovery rate (FDR) for peptides and proteins of <1%.

RESULTS

Mdc1 Thr-4 is a novel site of ATM phosphorylation *in vitro* and *in vivo*

Mdc1 contains many potential PI3 kinase-like protein kinase (PIKK) target sites (S/TQ-motives) throughout its open reading frame and early studies have shown that upon genotoxic stress, Mdc1 is rapidly phosphorylated in a PIKK-dependent manner (3–5). However, only few of these potential PIKK target sites are conserved and the extent and physiological relevance of PIKK-dependent Mdc1 phosphorylation are largely unknown. In order to identify *bona fide* PIKK target sites in Mdc1, we generated eight overlapping fragments of the human Mdc1 cDNA and expressed them in *E. coli* as GST-fusion proteins as described previously (13) (Figure 1a). All but one fragment (M-6) comprising the Mdc1 PST-repeat region, expressed well and could be purified (Figure 1a, upper panel). These fragments were then phosphorylated *in vitro* using immunoprecipitated human ATM (20). Surprisingly, ATM only phosphorylated fragment M-1 (amino acids 1–124) and fragment M-4 (amino acids 531–770) (Figure 1a, lower panel). Fragment M-4 features a cluster of four conserved 'T-Q-X-F' motifs that constitute binding sites for the FHA domain of the ubiquitin ligase RNF8 following phosphorylation by ATM (21–23). Fragment M-1 contains two conserved TQ motifs: one at the very N-terminus of Mdc1 (Thr-4/Gln-5) and one within the FHA domain (Thr-98/Gln-99). Thr-4 appears to be the major site of ATM phosphorylation since a deletion mutant of M-1 lacking the first 18 amino acids was not phosphorylated by ATM *in vitro* (Supplementary Figure S1), and a point mutation altering Thr-4 to Ala (T4A) resulted in a protein that could no longer be phosphorylated by ATM *in vitro* (Figure 1b).

In order to investigate Thr-4 phosphorylation *in vivo*, we raised a phosphor-specific antibody (pT4) directed against a pThr-4 peptide derived from the Mdc1 N-terminus. The antibody recognized the *in vitro* phosphorylated M-1 fragment and cross-reacted only minimally with the unphosphorylated form of M-1 and a T4A mutant M-1 fragment (Figure 1b, third panel). Moreover, the antibody did not recognize the repeating TQxF motifs within fragment M-4 (Supplementary Figure S2) either before or after ATM phosphorylation, indicating clear specificity for the pThr-4 site. We then exposed U2OS cells to various doses of IR and analyzed total cell extracts by immunoblotting with the pT4 antibody. The antibody cross-reacted with several proteins in total cell extracts, but one band (migrating at ~250 kDa) appeared only in extracts derived from cells that had been treated with IR (Supplementary Figure S3). The intensity of this band increased with increasing dose of IR (Figure 1c, left). Stripping and reprobing the blot with an antibody against human Mdc1 revealed that the protein recognized by the pT4 antisera overlapped with at least one of the Mdc1 isoforms. Time course analysis showed that 1 h post irradiation, phosphorylation levels were maximal and then slowly decreased to background levels after 21 h (Figure 1c, right panels). Moreover, in cells expressing a tagged T4A-mutated version of the Mdc1 N-terminus, only a very weak signal was detectable by the pT4 antibody, while the wild-type protein was readily detected (Supplementary Figure S4).

To exclude the possibility that the pT4 antibody cross-reacted with another protein phosphorylated in response to IR, we subjected Mdc1$^{-/-}$ mouse embryonic fibroblasts and control (Mdc1$^{+/+}$) cells to various doses of IR and analyzed total cell extracts by immunoblotting using the pT4 antibody. In extracts prepared from irradiated Mdc1$^{+/+}$ MEFs, a clear signal appeared on polyacrylamide gels at the position where mouse Mdc1 would be expected. No such signal was detected in extracts derived from irradiated Mdc1$^{-/-}$ cells, indicating that the protein recognized by the pT4 antibody indeed corresponds to Mdc1 (Figure 1d).

Mdc1 phosphorylation in response to IR is ATM dependent (3–5). Consistent with this, no Mdc1 signal was detected by the pT4 antibody in extracts from irradiated cells that had been pre-treated with a specific ATM

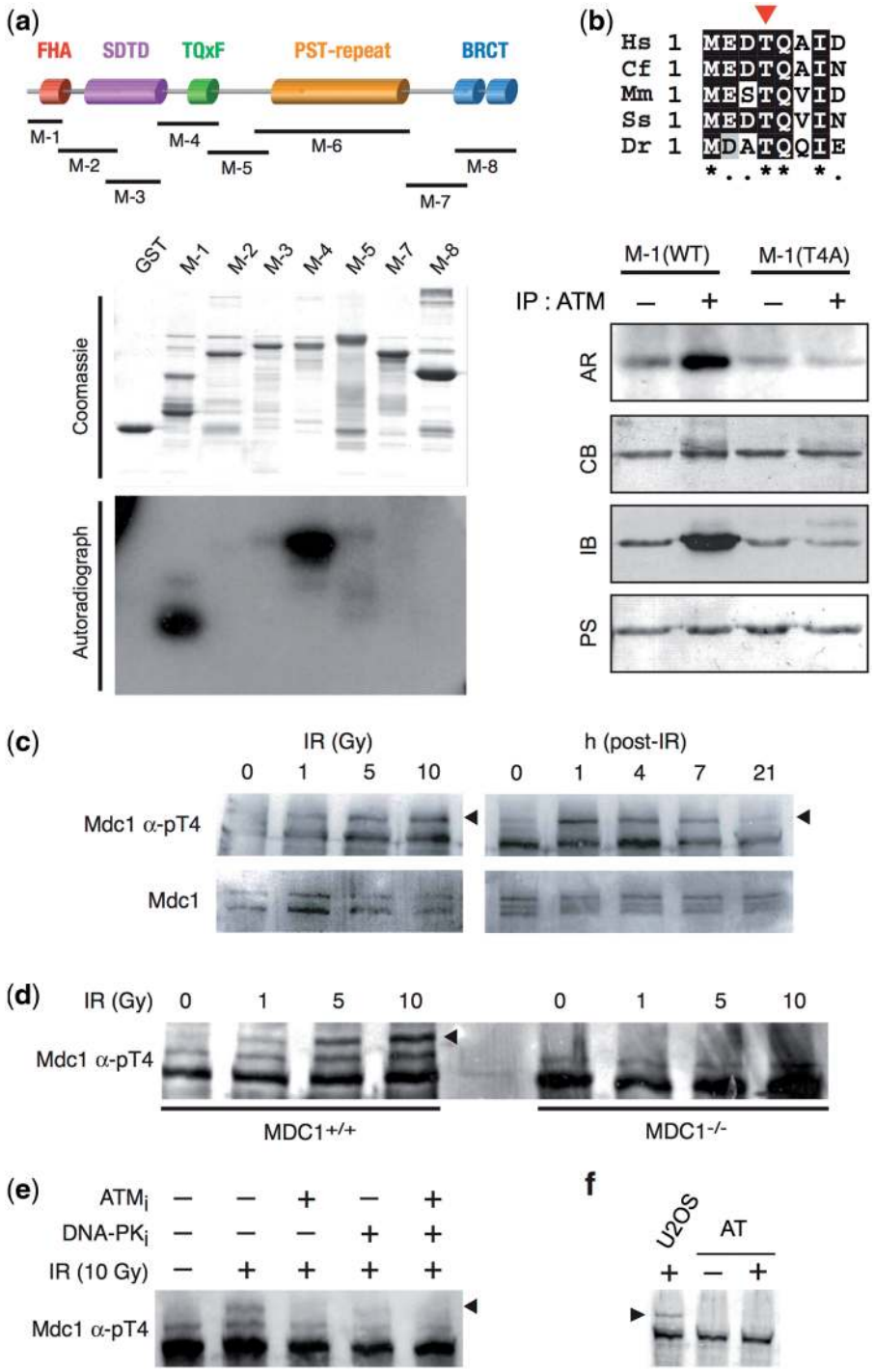

Figure 1. ATM targets Mdc1 on a conserved threonine residue at its N-terminus. (**a**) *In vitro* ATM kinase assay of recombinant Mdc1 fragments. Top: Schematic representation of Mdc1's domain architecture and of the GST-fusion fragments derived from its cDNA. Bottom: (Upper panel): Coomassie blue stained polyacrylamide gel of the purified GST-fusion fragments. (Bottom panel) Autoradiography of *in vitro* phosphorylated Mdc1 fragments. (**b**) A conserved motif at the very N-terminus of Mdc1 is phosphorylated by ATM *in vitro*. Top: Sequence alignment of the Mdc1 N-terminus. The highly conserved Thr residue at position 4 (T4) is highlighted by an arrowhead. (Bottom) ATM phosphorylation of fragment M-1 and the mutant T4A. AR, Autoradiograph; CB, Coomassie blue; IB, immunoblot; PS, Ponceau red. (**c**) (Left panel) Dose titration using the pThr-4 phosphospecific antibody (pT4). (Right panel) Kinetics experiment using the pT4 phosphospecific antibody. The band corresponding to Mdc1 is highlighted by an arrowhead. (**d**) $Mdc1^{+/+}$, $Mdc1^{-/-}$ MEFs were irradiated with various doses of IR. Extracts were probed with the pT4 antibody. (**e**) Mdc1 Thr-4 phosphorylation in response to IR is ATM-dependent. U2OS cells were pre-treated with highly specific inhibitors of ATM (KPL0064: Kudos), DNA-PKcs (NU7026: Kudos) or a combination of both. Cell extracts were probed with the phosphospecific pT4 antibody. (**f**) Mdc1 is not phosphorylated in cells derived from an A-T patient. A-T cells and control U2OS cells were irradiated and extracts were probed with the pT4 antibody.

inhibitor or with a combination of ATM and DNA-PKcs inhibitors, while the signal was still present, albeit weaker, when the cells had been pre-treated with the DNA-PKcs inhibitor alone (Figure 1e). In addition, no Mdc1 signal was detected by the pT4 antibody in extracts prepared from irradiated A-T cells (Figure 1f). Together, these data show that Mdc1 contains a conserved PIKK target site at its very N-terminus and that, in response to IR, this is mainly targeted by ATM *in vivo*.

The phosphorylated N-terminus of Mdc1 binds to its own FHA domain

To understand the functional implication of Mdc1 Thr-4 phosphorylation, we carefully analyzed the amino acid sequence surrounding the PIKK target site. Besides the TQ motif, several additional amino acids are conserved, most notably an isoleucine three residues C-terminal to the phosphoacceptor threonine (Figure 1b). This is intriguing since pT-X-X-I was previously shown to constitute a favored motif for certain classes of FHA domains (24). Indeed, the entire N-terminal motif (M-E-D-pT-Q-A-I) resembles that derived for the Mdc1 FHA domain by oriented library screening in these earlier studies (Figure 2a). In order to test whether the phosphorylated N-terminus of Mdc1 could serve as a binding site for an FHA domain-containing protein, we designed a phosphopeptide comprising the first 12 N-terminal residues of human Mdc1 phosphorylated on Thr-4. The phosphopeptide and its unphosphorylated derivative were coupled to magnetic beads and used to pull-down proteins from HeLa nuclear extracts. Both peptides retrieved several proteins that appeared as clear bands on a SDS–polyacrylamide gel (Supplementary Figure S5), but at least three proteins were pulled down by the phosphopeptide only, but not by its unphosphorylated counterpart. Most prominent were two bands of ~250 kDa identified as Mdc1 itself by western blot analysis with an antibody against human Mdc1 (Figure 2b). The other two bands at ~150 and ~80 kDa were RAD50 and MRE11, respectively. Together with our previous finding that Mdc1 exists in a complex with MRN in HeLa nuclear extracts (8,13), these results indicate that Mdc1 may be the predominant interaction partner of its own phosphorylated N-terminus.

Of the two phosphor-specific protein binding domains within Mdc1 (Figure 1a), phosphopeptide pull-down experiments with bacterially expressed GST-fusion proteins of these regions showed that only the FHA domain bound tightly and specifically to the Mdc1 N-terminal phosphopeptide, with no significant interaction detectable for the C-terminal BRCT-repeat region (Figure 2c). Furthermore, we were able to demonstrate high affinity binding of purified Mdc1 FHA to a synthetic phosphopeptide encompassing the Thr-4 motif by isothermal titration calorimetry (ITC) (Figure 2d). Interestingly, these data could only be satisfactorily fit using a model incorporating two independent phosphopeptide binding sites (see below).

In order to confirm these interpretations in an unbiased manner, we performed a SILAC-based screen for interaction partners of the Mdc1-FHA domain by mass spectrometry that is further described later. Importantly, analysis of protein complexes pulled down by the overexpressed Mdc1 FHA domain revealed a clear interaction with endogenous Mdc1 and Mdc1 phosphorylation on Thr-4 could be unambiguously confirmed (Figure 2e). Furthermore, Stable Isotope Labelling with Amino-acids in Cell culture (SILAC) and extracted ion chromatogram-based quantitation (25) of the signal abundances of phosphorylated and unphosphorylated Thr-4 peptides from a similar SILAC screen reveals an increase in intensity-dependent occupancy rate for the phosphorylated Thr-4 peptide from 18.6% to 61.5% after irradiation. While the unphosphorylated form of the second possible ATM site, Thr-98, was detected, no phosphorylated form was evident (Supplementary Figure S6a). Significantly, Thr-98 occurs within an Asn-Gly-*Thr*/Val or 'NGT' motif conserved in a majority of FHA domains. Here, it packs into the protein core and structurally supports the preceding asparagine residue that, in turn, makes crucial hydrogen-bonding contacts with main-chain atoms from bound phosphopeptides (ref. 24; and this paper). Together, these observations have implications for a recently proposed mechanism of Mdc1 oligomerization through FHA binding to pThr-98 (26).

Interestingly, we could not detect peptides for ATM, Rad51 or Chk2 in the protein fraction pulled down by the Mdc1–FHA domain, even though these three proteins have previously been proposed to interact directly with the Mdc1–FHA domain (3,9,10,12). We were also unable to detect ATM or Chk2 in these fractions by western blot analysis (Supplementary Figure S6b) and no interaction of purified Mdc1–FHA domain with a phosphopeptide containing ATM pSer-1981 motif by ITC was observable (Supplementary Figure S6c). This contrasts with previous observations of this interaction by other methods (10) but the lack of binding is wholly consistent with a generally accepted view that FHA domains are pThr specific.

The Mdc1–FHA domain forms a dimer

In order to characterize the Mdc1–FHA–pThr 4 interactions further, we determined the structures of both free and phosphopeptide-bound forms at high resolution by X-ray crystallography. The pThr-4 phosphopeptide complex structure was solved using the single wavelength anomalous diffraction method with crystals grown from selenomethionine-substituted Mdc1–FHA domain, and a synthetic peptide in which Ala-6 was also replaced by selenomethionine, an approach we have described previously (27). The refined coordinates of the complex were then used to solve the structure of the peptide-free form by molecular replacement. Data collection and refinement statistics are shown in Table 1 along with representative electron density for residues at the edge of the FHA dimer interface (Figure 3a).

As expected, the Mdc1–FHA domain adopts an 11-stranded β-sandwich fold that is characteristic of these signaling modules (Supplementary Figure S7). Strikingly, we observed two FHA domains in the asymmetric unit in both peptide-free and bound forms, each similarly arranged around a pseudo 2-fold

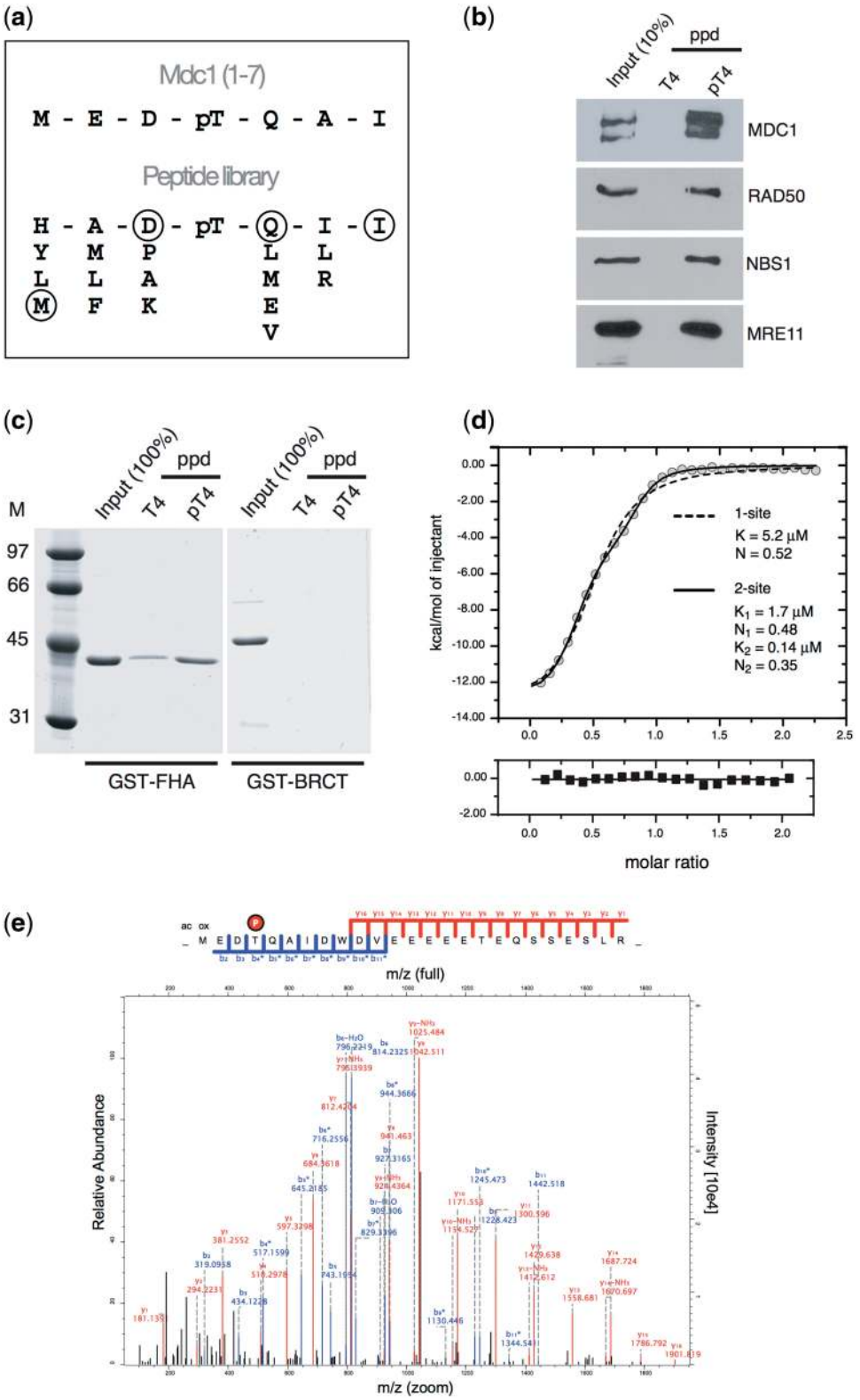

Figure 2. The phosphorylated Mdc1 N-terminus constitutes a recognition motif for the Mdc1–FHA domain. (**a**) The N-terminal Mdc1 pThr-4 sequence closely resembles the optimal binding motif derived previously (24) by oriented peptide library selection. Circled residues highlight exact matches. (**b**) Immunoblot analysis indicates that endogenous Mdc1 is efficiently pulled down by the pThr-4 phosphopeptide. (**c**) Coomassie blue-stained PAGE of a pThr-4 phosphopeptide pull-down experiment using purified M-1 GST-fragment (containing the FHA domain) and purified M-8 GST-fragment (containing the BRCT domains). (**d**) Upper panel—ITC binding isotherm for interaction of a phosphorylated (upper) or non-phosphorylated (lower) synthetic Thr-4 peptide with recombinant Mdc1–FHA domain. Data were analyzed assuming one or two site binding which consistently favored the latter model, showing tight, stoichiometric (1:1) binding to similar but non-identical sites. (**e**) Representative MS ion fragment spectra of the N-terminal Mdc1 tryptic peptide showing phosphorylation at Thr-4 acquired with high mass accuracy (ppm) and a false discovery rate (PEP) below 1%.

Table 1. Crystallographic statistics

	Mdc1/pThr-4 (Se SAD)	Mdc1
Data collection		
PDB ID	3UOT	3UN0
Space group	$P2_12_12_1$	$P2_12_12_1$
Cell dimensions (Å)		
a, b, c (Å)	58.5, 59.9, 72.1	35.3, 54.7, 98.1
	Peak	
Wavelength (Å)	0.9790	
Resolution (Å)[a]	15.0–1.8 (1.86–1.80)	20.0–2.3 (2.40–2.30)
R_{merge} (%)	3.7 (31.5)	8.4 (40.4)
$<I/\sigma(I)>$	27.5 (2.1)	11.7 (2.8)
Completeness (%)	93.4 (55.3)	93.7 (90.2)
Redundancy	3.2 (2.1)	3.0 (2.9)
Refinement		
Resolution (Å)	15–1.8	15.0–2.3
No. of reflections	21 805	7988
R_{work}/R_{free} (%)	20.5/24.3	20.7/26.1
No. of atoms		
Protein	1757	1699
Peptide	142	–
Water	150	79
Sulphate	–	7
B-factors (Å^2)		
Protein	25.4	39.2
Peptide	45.0	–
Water	41.2	50.8
R.m.s deviations		
Bond lengths (Å)	0.01	0.009
Bond angles (°)	1.5	1.5
Ramachandran plot (%)		
Favored	225 (97.4)	199 (94.3)
Allowed	5 (2.2)	10 (4.7)
Disallowed	1 (0.4)	2 (1)

[a]Values in parentheses are for highest resolution shell.

non-crystallographic symmetry axis (Figure 3b and Supplementary Figure S8). Although other FHA–FHA lattice interactions are observed in the two crystal forms, the non-crystallographic interaction surface is the most extensive burying a total of ~900Å^2/dimer in each case. Of these, ~600Å^2 are contributed by non-polar atoms from the side-chains of Phe-37, Leu-101, Leu-120, Leu-122 and Leu-127 (Figure 3c), all highly conserved in available sequences of Mdc1 orthologs (Figure 3d). Together these residues form a hydrophobic cluster on one face of each FHA β-sandwich that is tightly packed with high surface complementarity at the interface.

In the light of these observations, we examined the solution behavior of the isolated FHA by size-exclusion chromatography combined with multi-angle laser light scattering (SEC-MALLS) that is able to conveniently measure shape independent and accurate molecular weights from chromatographic peaks, circumventing the need for analytical ultracentrifugation analysis. The molar mass distribution across the chromatographic peak showed an apparent molecular weight of 18.3 ± 0.06 kDa, some 40% greater than the calculated monomer mass of 12.8 kDa unambiguously demonstrating self-association of the Mdc1–FHA domain (Figure 3e). Moreover, a double mutation, L120E/L127E, resulted in a significant reduction in apparent molecular weight (14.3 kDa; Figure 3e) presumably due to juxtaposition of repulsive charges at the interface. Thus, we conclude that the dimeric arrangement observed in the crystal structures is indeed representative of the dimer we observe in solution.

Thr-4 phosphorylation stabilizes Mdc1–FHA domain dimerization

The structure of the Mdc1–FHA/phosphopeptide complex (Figure 4a) shows a binding mode for the pThr-4 motif resembling that seen in many previously reported FHA domain complexes (28). The phosphothreonine is held by a network of hydrogen bonds with the highly conserved Arg-58 and Ser-72 side-chains along with accessory interactions with Lys-73 (Figure 4b). Ile-7 occupies the pThr +3 position that has been shown to represent a major determinant of FHA specificity (18) and interacts with the FHA domain through a shallow pocket. Interestingly, Trp-9 that is present in all available sequences of Mdc1 orthologs is the last peptide residue visible in electron density maps and sits in a cleft formed at the edge of the FHA–FHA interface. Since the local 2-fold symmetry is imperfect, the FHA domain interactions of the Trp-9 side-chain from the non-crystallographic symmetry-related peptide are still significant but less extensive, potentially explaining the two binding sites apparent in ITC measurements. Regardless, the structural data strongly suggest that pThr motif binding might contribute to the overall stability of the dimeric complex and further SEC-MALLS analysis (Figure 4c) clearly showed that addition of the pThr-4 peptide substantially increases the apparent weight-averaged molecular weight to within ~90% of that calculated for a fully dimeric, peptide-bound complex. Consistent with the structural location of Trp-9 at the FHA–FHA interface, a peptide variant containing a W9A substitution results in no significant dimer stabilization.

These data reveal a dimeric FHA domain architecture that is stabilized through binding of each FHA domain *in trans* to a motif representing the ATM-phosphorylated Mdc1 N-terminal region. In support of this idea, we note that the conserved and highly acidic region (residues 10–18) C-terminal to Thr-4 could potentially interact with an equally conserved basic patch adjacent to the pThr-4 binding site but located on the adjacent protomer of the Mdc1 dimer (Figure 4d). Nonetheless, we realized that other arrangements are possible when the N-terminal motif is covalently attached to the FHA through the intervening linker region (Figure 4e). In particular, the peptide-binding data did not eliminate the possibility of polymerization of the intact molecule, nor did they exclude intra-molecular binding of the phosphorylated N-terminal motif to its own FHA domain as we have observed previously for the Rv1827 FHA-domain protein from *Mycobacterium tuberculosis* (29). In order to distinguish between these possibilities, we used expressed protein ligation technology to generate a specifically and stoichiometrically Thr-4-phosphorylated sample (Figure 4f, left panel) as we had

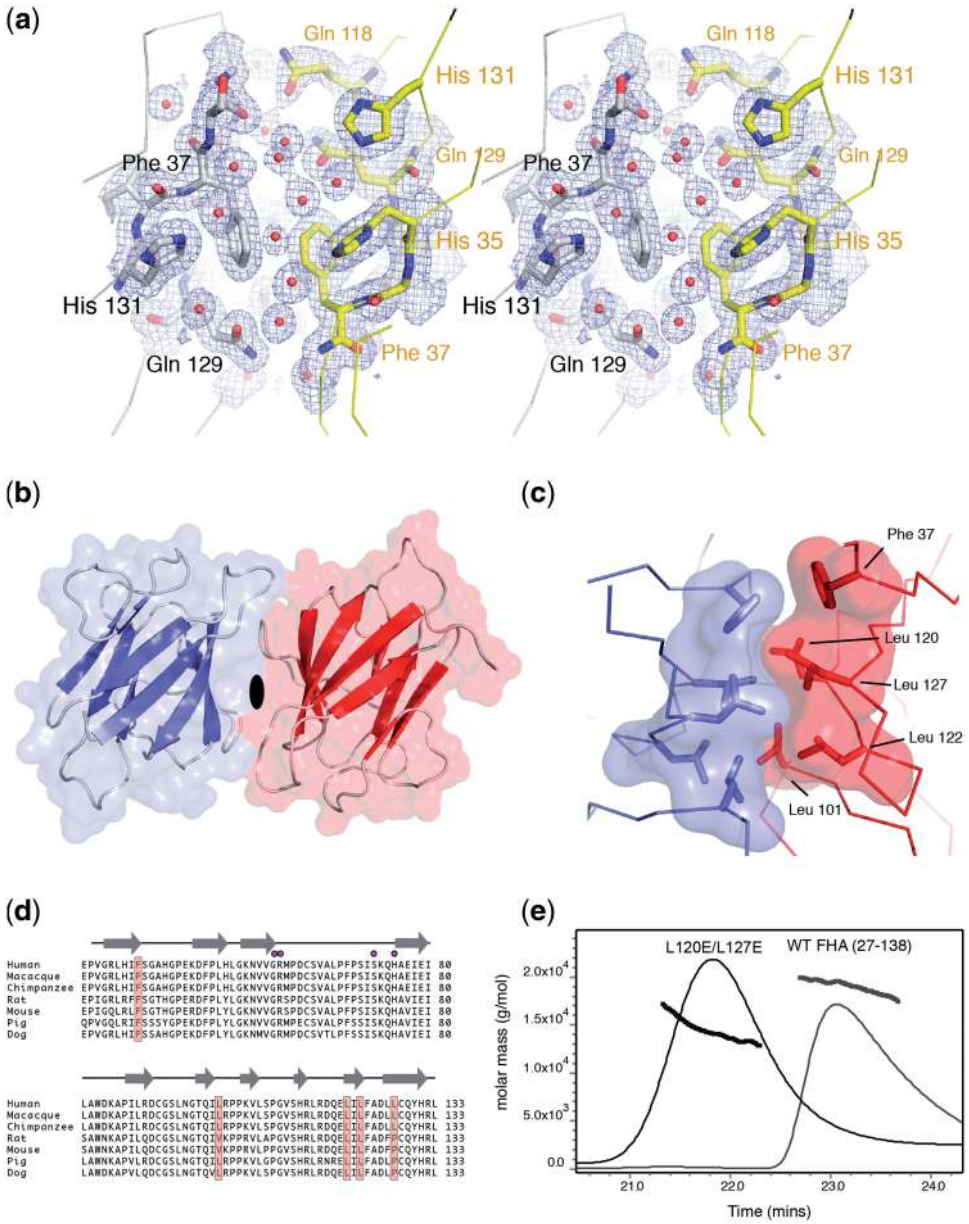

Figure 3. Mdc1–FHA domain dimerization. (**a**) Stereo view of a segment of omit electron density map (1.25σ) at the periphery of the FHA–FHA interface from the 1.8 Å resolution peptide complex. Protein residues are shown as stick representation and water molecules are shown as red spheres. (**b**) Ribbons representation of the dimeric arrangement observed in the peptide-free Mdc1–FHA crystal structure. The position of the local 2-fold symmetry axis is indicated. All structural representations were generated using PyMOL (http://pymol.sourceforge.net/). (**c**) FHA–FHA interactions are predominantly mediated by a conserved cluster of five hydrophobic residues from each protomer. (**d**) Interface residues are highly conserved in all available sequences of Mdc1 orthologs. The locations of β-strands observed in the structure are indicated in the lower panel, along with the positions of the four residues most highly conserved in the FHA domain family (circles). (**e**) SEC-MALLS analysis of the wild-type Mdc1–FHA (27–138) and a mutant form in which two residues that form the core of the observed dimer interface have been substituted with glutamate. The observed weight-averaged molecular weight of the mutant is substantially less than the wild-type protein. The shorter retention time for the mutant may reflect a more extended shape for monomeric forms, or differential electrostatic effects on interaction of the mutant with the weakly anionic column matrix. Thin lines, UV absorbance; thick lines, derived molar mass distributions across the chromatogram peak.

done previously for Chk2 (30). SEC-MALLS analysis of this molecule reported an apparent molecular weight of 31.2 kDa, essentially identical to the formula mass of the fully dimeric phosphorylated fragment (31 110 Da) (Figure 4f, right panel). Thus, we conclude that pThr-4 phosphorylation results in tight Mdc1 dimerization through a head-to-tail mechanism.

Mdc1 self-association occurs in human cells and is pThr-4-dependent

We next asked whether the head-to-tail dimer also occurs in human cells. First, we used differentially tagged Mdc1 fragments to detect homotypic interaction by co-immunoprecipitation. As shown in Figure 5a, a

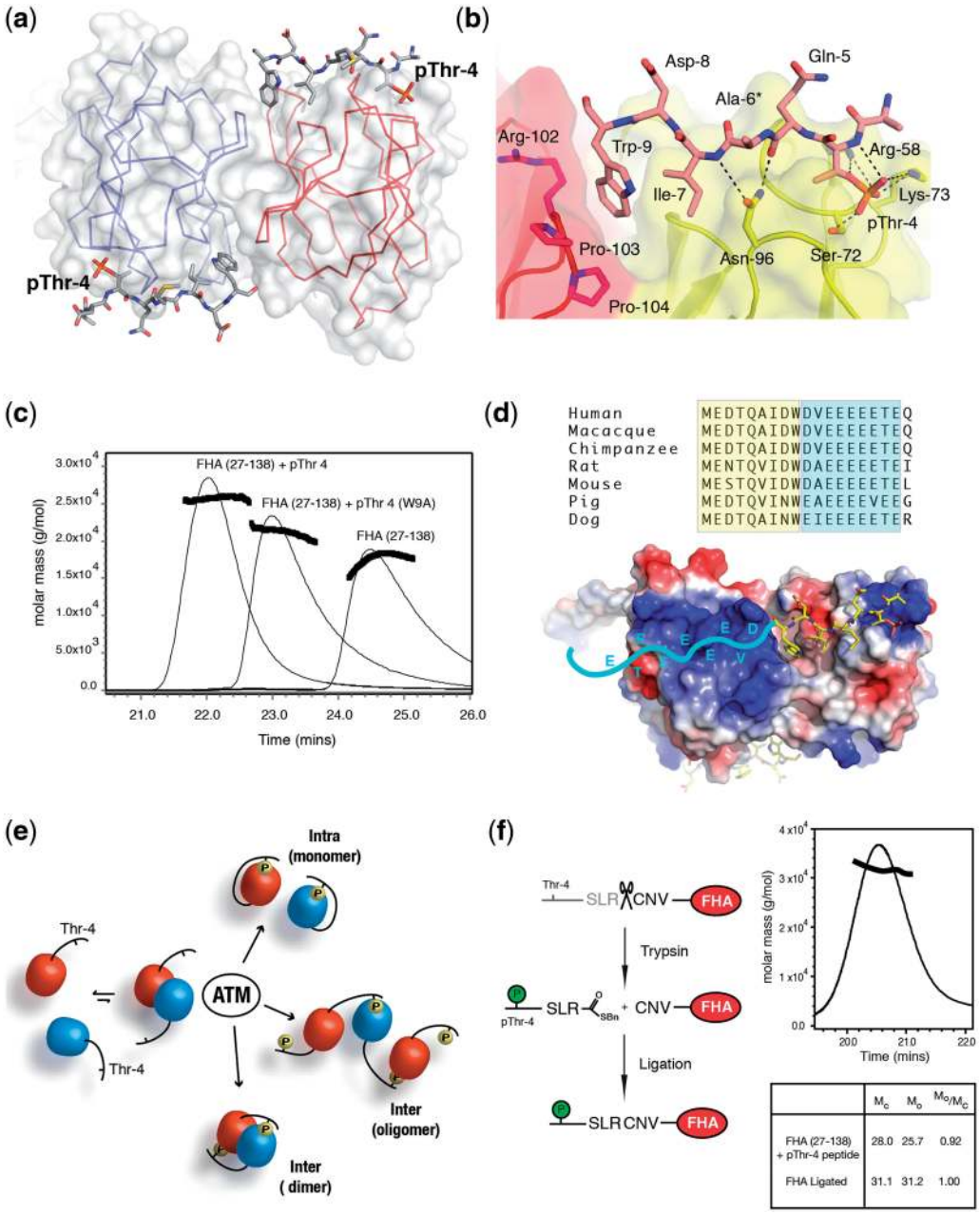

Figure 4. Head-to-tail dimerization is stabilized by pThr-4. (**a**) Structure of the Mdc1/pThr-4 peptide complex is shown as a Cα plot/surface representation with the peptide shown as sticks, viewed along the local 2-fold symmetry axis. (**b**) The phosphopeptide interacts with conserved FHA domain residues mainly through pThr-4 and main-chain atoms from pT + 1 and +3 residues. The Trp-9 indole nestles in a cleft formed at the interface between the two FHA domains in the dimer. (**c**) SEC-MALLS analysis shows that a substantial stabilization of the Mdc1–FHA dimer by the pThr-4 peptide is greatly reduced by substitution of Trp-9 with alanine (W9A). The slight differences in retention times of the peptide-free wild-type FHA observed in this experiment and that of Figure 3c arise from small differences in the on-column concentration (typically ±3–4%), the weak self-association of the unphosphorylated molecule and the fact that peak concentrations are of the same order as the estimated dimerization affinity. (**d**) The sequence C-terminal to the pThr-4 motif (yellow) contains a highly conserved stretch of acidic residues highlighted in blue (top panel). These would be predicted to interact with arginine and lysine residues that are also conserved and form a basic patch adjacent to the binding site for the peptide C-terminus of the bound peptide (bottom). (**e**) Cartoon showing the three most likely effects of Thr-4 phosphorylation. (**f**) Ligation of an extended pThr-4 peptide to trypsin-cleaved Mdc1–FHA (left) produces a stoichiometrically and specifically phosphorylated protein encompassing the entire N-terminal region that forms a tight dimer by SEC-MALLS analysis (right). M_o, observed molecular weight; M_c, calculated molecular weight.

Flag-tagged Mdc1 fragment (1–800) efficiently interacted with an identical Myc-tagged fragment. An N-terminal Mdc1 fragment lacking the BRCT domains was used to avoid avid association of Mdc1 with DNA damage-induced chromatin. Surprisingly, interaction between the two fragments was not completely dependent on IR treatment. However, we noticed that transiently expressed Mdc1 (1–800) fragment was constitutively

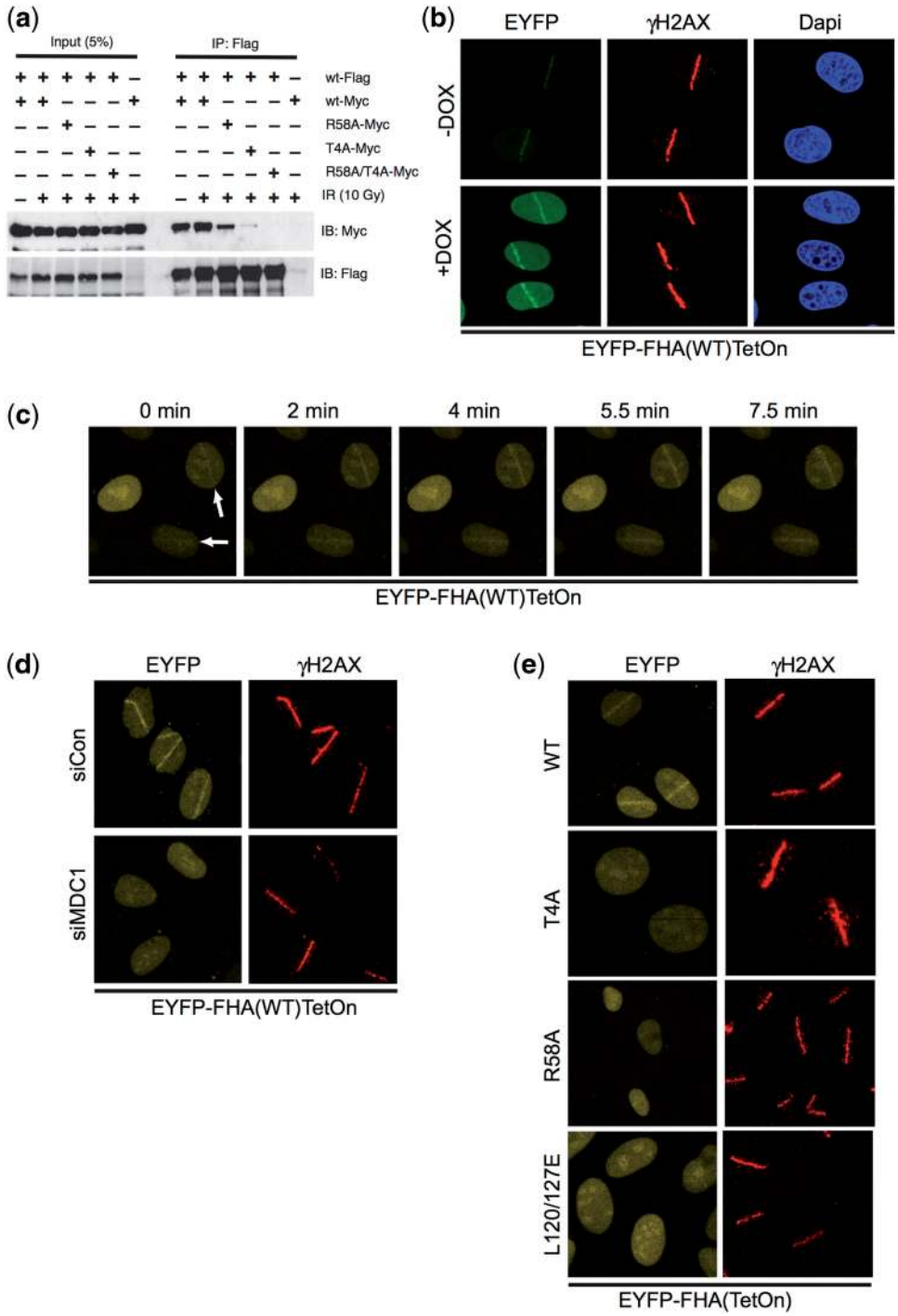

Figure 5. Dimerization of the Mdc1 N-terminal region *in vivo*. (**a**) The interaction between differentially tagged Mdc1 N-terminal fragments is dependent upon the intact FHA domain and Thr4 phosphorylation. 293T cells were transiently transfected with Flag-tagged Mdc1 (1–800 amino acids) and Myc-tagged Mdc1 (1–800 amino acids) wild-type and the indicated mutants, respectively. Protein complexes were immunoprecipitated with monoclonal anti-Flag agarose and immunoblotted with polyclonal anti-Myc and polyclonal anti-Flag antibodies. (**b**) The Mdc1–FHA domain is recruited to damaged chromatin regions. U2OS expressing a tetracycline-inducible EYFP–FHA $(WT)^{TetOn}$ fusion protein were treated with doxocyclin for 1 h and subjected to laser irradiation. Cells were fixed 30 min after irradiation and immunostained for γH2AX. (**c**) Kinetics of Mdc1–FHA domain recruitment. U2OS FHA (WT)-$EYFP^{TetOn}$ cells were incubated with doxocycline for 1 h and subjected to laser irradiation. Time lapse live cell microscopy was performed and images were taken at the indicated times. Note that for technical reasons, 0 min time point was taken about 20 sec after microirradiation. (**d**) Recruitment of Mdc1–FHA domain is dependent on endogenous Mdc1. U2OS FHA(WT)$EYFP^{TetOn}$ cells were either treated with control siRNA or siRNA against endogenous Mdc1. Cells were induced with doxocycline for 1 h, subjected to laser irradiation and images were taken 30 min thereafter. Cells were subsequently fixed and immunostained for γH2AX. (**e**) Recruitment of Mdc1–FHA domain is dependent on phospho-specific interaction between Thr4 and the FHA domain as well as on an intact hydrophobic interface between FHA monomers. U2OS FHA-$EYFP^{TetOn}$ cells expressing the wild-type and indicated mutants were induced with doxocyclin for 1 h, subjected to laser irradiation and images were taken 30 min thereafter. Cells were subsequently fixed and immunostained for γH2AX.

phosphorylated on Thr-4 even without prior irradiation of the transfected cells (data not shown). Since Thr-4 phosphorylation of endogenous Mdc1 is clearly DNA damage dependent (Figure 1), we assume that this effect is a result of the transfection procedure (31). Nevertheless, a moderate increase in the interaction could be detected upon treatment of cells with IR (Supplementary Figure S9a). In addition, the Mdc1 (1–800) fragment co-immunoprecipitated with endogenous Mdc1 exclusively in extracts prepared from IR-treated cells (Supplementary Figure S9b). Crucially, mutation of either the FHA domain (R58A) or a T4A substitution led to a significant reduction of the interaction between Flag-tagged and Myc-tagged Mdc1 (1–800) and concomitant mutation of both the FHA domain and Thr-4 resulted in a complete loss of binding (Figure 5a). To eliminate the possibility that one or both of the other two classes of known pThr-containing phosphorylation sites within Mdc1—pSDpTD (13,32–34) and pTQxF (21,23)—were contributing to interactions of the Mdc1 (1–800) FHA domain we carried out ITC titrations of the recombinant Mdc1–FHA with synthetic versions of these phosphomotifs. No detectable interactions were observable in either case (Supplementary Figure S10).

On the basis of these experiments, we reasoned that if DNA damage-induced Mdc1 dimerization occurs via the FHA domain, we should detect partial recruitment of the FHA domain to sites of DSBs through association with endogenous Mdc1. Moreover, this recruitment should be diminished by mutations in either the FHA domain or at the pThr-4 site. To circumvent limitations of the static assessment of IRIF formation in fixed cells, we used an integrated imaging unit that combines microlaser-assisted generation of spatially defined DSB areas in mammalian cells with rapid, continuous and interactive image acquisition (35,36). Since it has been previously observed that overexpression of the Mdc1–FHA domain interferes with accumulation of DDR proteins (including Mdc1 and the Mre11/Rad50/Nbs1 complex) at sites of DSBs (5,11,37), we also generated a panel of cell lines derived from checkpoint-proficient U2OS cells carrying stably integrated, tetracycline-regulated expression cassettes directing the expression of the Mdc1–FHA domain fused to enhanced yellow fluorescent protein (EYFP). Significantly, when expressed at low levels, the Mdc1–FHA domain is recruited to microlaser-induced DNA damage (Figure 5b). The real-time measurements revealed a rapid accumulation of the fusion protein around the laser generated, DSB-containing, subnuclear tracts (Figure 5c), with a detectable increase in fluorescence in the damaged nuclear compartments within 20–30 s (Figure 5c, first panel). Subsequently, the fusion protein underwent a rapid accumulation in the DSB regions, and reached a steady-state by 8–10 min after laser exposure. Importantly, no increase in fluorescence was observed in DSB-containing laser tracks in Mdc1-depleted cells, indicating that EYFP–FHA domain accumulation is strictly dependent on endogenous Mdc1 (Figure 5d). Moreover, no accumulation was detectable in cells that express T4A or the R58A and L120/127E mutant derivatives of the FHA domain (Figure 5e). Thus, these data reveal that FHA accumulation to microlaser-induced DNA damage in living human cells mirrors the *in vitro* requirements for Mdc1 dimerization, strongly supporting the notion that Mdc1 dimerization in response to DNA damage also occurs *in vivo* and that is does so in a manner that is consonant with our structural data.

Mdc1 dimerization does not influence Mdc1 recruitment or 53BP1 localization to sites of DNA double-strand breaks

It was previously demonstrated that overexpression of the Mdc1–FHA domain yields a dominant-negative impact upon Mdc1 accumulation at sites of DNA damage (5,37,38). Thus, we sought to investigate whether FHA-mediated Mdc1 dimerization was required for optimal recruitment of full-length Mdc1 to sites of DNA damage. To this end, we generated stable U2OS cell lines expressing GFP-tagged versions of full-length wild-type Mdc1 or T4A mutant Mdc1 (Supplementary Figure S11). Both quantitative real-time imaging on microlaser-induced DNA damage tracks in living cells (Supplementary Figure S12a) as well as immunofluorescence analysis on IR-treated fixed cells (Supplementary Figure S13) revealed that the T4A mutation had no influence on full-length Mdc1 recruitment to sites of DSBs.

Since it has also been recently suggested that DNA damage-induced Mdc1 oligomerization, presumably through the mechanism that we describe, is required for 53BP1 accumulation at sites of DNA damage (39) we also analyzed the effect of the Mdc1 T4A mutation on 53BP1 foci formation. We transiently transfected $Mdc1^{-/-}$ mouse embryonic fibroblasts with full-length HA-tagged mouse Mdc1 (wild-type or T4A mutant) and assessed 53BP1 foci formation after irradiation by immunofluorescence. Even though a subtle (but reproducible) reduction of the number of cells with 53BP1 foci was detectable in the T4A-expressing cells as compared to wild-type-expressing cells (Supplementary Figure S12b), 53BP1 foci formation appeared to be relatively normal in most reconstituted $Mdc1^{-/-}$ MEFs, suggesting that FHA-mediated Mdc1 dimerization is not essential for 53BP1 accumulation, although it may contribute to its regulation.

A screen for interaction partners of the Mdc1–FHA domain

Finally, in order to directly investigate Mdc1–FHA interactions in human cells, we designed an unbiased and quantitative proteomic analysis of Mdc1–FHA interaction partners in the presence and absence of DNA damage. SILAC-labeled U2OS cells stably expressing an empty control plasmid or a Strep-tagged Mdc1–FHA domain (amino acids 1–154) were irradiated with 10 Gy of IR or left untreated. FHA-interacting proteins were then pulled down by Strep-Tactin Sepharose and eluted from the beads. The eluates were combined, digested with trypsin and analyzed by high-resolution LC–MS/MS (Figure 6a). The Mdc1–FHA interaction 'affinities' were determined by a quantitative comparison of tryptic peptide abundances (Figure 6b). Each tryptic peptide occurred as a

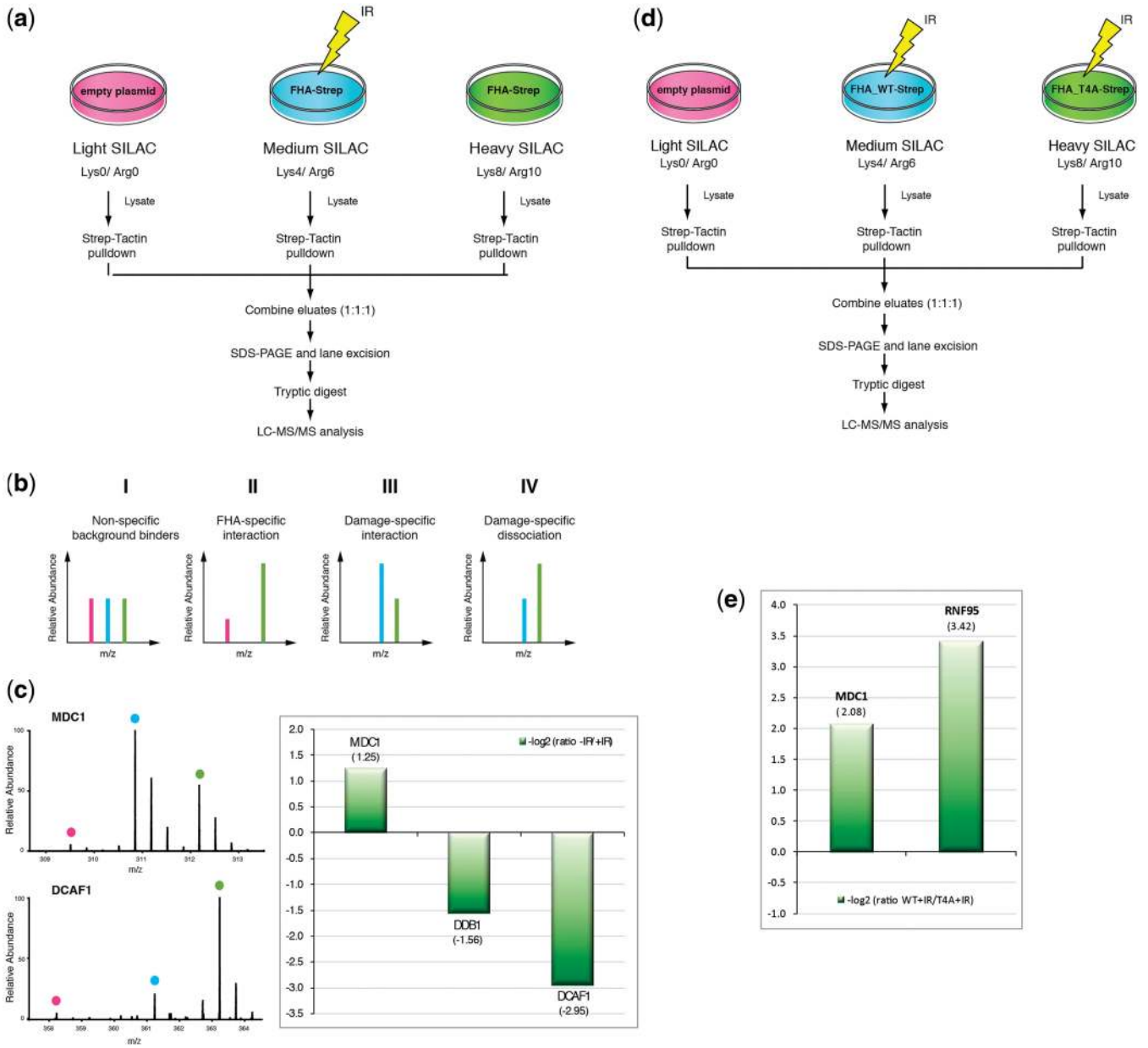

Figure 6. SILAC analysis FHA-dependent interactions of Mdc1. (**a**) Experimental scheme of the quantitative analysis of MDC1–FHA domain interaction partners. (**b**) Schematic representation of the interpretation of quantitative SILAC data. (**c**) DNA damage-dependent interaction partners of the MDC1–FHA domain. (Left) Survey full scan MS spectrum of an MDC1 peptide showing a SILAC ratio, which corresponds to a damage-increased interaction with the MDC1–FHA domain whereas the SILAC ratio of a DCAF1 peptide shows a ratio indicating a damage-specific dissociation. (Right) Normalized $\log_2$ SILAC ratios (−IR/+IR; 10 Gy, 30 min) for MDC1, DDB1 and DCAF1 as quantified by the mass spectrometric MDC1–FHA pull-down experiment. (**d**) Experimental scheme of the quantitative analysis of MDC1–FHA domain interaction partners in response to IR using over expressed MDC1–FHA WT and T4A mutant domains. (**e**) Dimerization-dependent interaction partners of the MDC1–FHA domain. Normalized $\log_2$ SILAC ratios (WT + IR/T4A + IR; 10 Gy, 30 min) for MDC1 and RNF95 as quantified by the mass spectrometric MDC1–FHA pull-down experiment.

SILAC triplet. If the SILAC peptide intensity ratio between light, medium and heavy peaks is 1:1:1 the identified protein was considered a background binder (Scenario I). Proteins significantly enriched in heavy isotope encoded samples show high SILAC ratios, and hence were considered Mdc1–FHA-specific interaction partners (Scenario II). Proteins enriched in IR-treated SILAC state were regarded as damage-specific FHA interaction partners (Scenario III), while proteins only enriched in untreated SILAC state were regarded as damage-specific dissociating proteins (Scenario IV).

As expected, the data revealed that Thr-4 phosphorylation of the Mdc1–FHA fragment used as bait in this screen increased substantially upon IR treatment (Figure 2e). Moreover, quantitative comparison of tryptic peptide abundances revealed endogenous Mdc1 as a DNA damage-specific interaction partner of its own FHA domain as predicted from our biochemical,

structural and cell-biological data. Interestingly, DDB1 (DNA damage binding protein 1) and DCAF1 (DDB1- and Cul4-associated factor 1), two proteins that occur in a Cul4-dependent ubiquitin ligase complex showed a significant (>2.5-fold) decreased interaction with the MDC1–FHA domain in the presence of DNA damage, thus suggesting that the Cul4/DDB1/DCAF1 complex may dissociate from MDC1 upon induction of DNA damage (Figure 6c).

Finally, a further screen to investigate IR-specific interactions indicated by the initial wild-type FHA analysis was carried out using plasmid only control cells alongside IR-treated cells expressing either wild-type or T4A mutant FHA domain (Figure 6d). As expected, endogenous Mdc1 interacts with the wild-type fragment consistent with stabilization of binding by head-to-tail dimerization. However, these data additionally showed that interactions with an uncharacterized RING-finger domain protein, RNF95, were also significantly increased in the wild-type compared to T4A FHA domain expressing cells (Figure 6e) suggesting FHA domain dimer-specific binding.

DISCUSSION

Mediator proteins perform a variety of crucial roles in many, if not all aspects of the response to DNA damage. Although these molecules are essentially unrelated, oligomerisation now appears to be core feature of their activities and 53BP1, along with budding yeast Rad9 and fission yeast Crb2 have all been shown to self-associate albeit through different mechanisms (40–45). Here, we have presented a comprehensive molecular description of a novel, FHA-mediated dimerization mechanism used by archetypal mediator Mdc1 in response to ATM phosphorylation following DNA damage.

A general role for dimerization in FHA domain signaling

Our observation of phospho-independent FHA dimerization is intriguing. Previous sequence comparisons have identified a patch of low-level conservation associated with β-strands 9 and 10 and the connecting loop of a subset of FHA domains, leading to the suggestion that this may act as a self-interaction surface (46). Our structure now shows that this putative surface substantially overlaps with the Mdc1 dimer-forming region (Supplementary Figure S14) and we also show that mutations within this region disrupt FHA–FHA interactions *in vitro* (Figure 3d) and in living human cells (Figure 5e). These and our previous data (29), support a more expansive role for the β-sandwich architecture in FHA-mediated interactions than has previously been envisaged.

Mdc1-like dimerization in Chk2/Rad53 family kinase activation

Previous studies have suggested that ATM-phosphorylated (pThr-68) Chk2 kinase constitutes a pre-activated, dimeric state (30,47) in which the pThr-68 motif of each protomer binds to the FHA domain of the other, bringing the kinase domains together for T-loop phosphorylation *in trans*. Indeed, X-ray structures of un-phosphorylated FHA/kinase domain-containing versions of Chk2 (48) show that the weak self-association of the isolated Chk2 FHA domain (30) occurs through interactions that are closely related to those seen in our Mdc1 structure in spite of substantial divergence at the sequence level (Supplementary Figure S15a). We further note that the two FHA domains that comprise the asymmetric unit of our earlier crystal structure of an FHA–phosphopeptide complex from the Chk2 ortholog, Rad53 (24) (PDB: 1G6G), show an almost identical dimeric interaction, strongly suggesting that the activation mechanism of human Chk2 is conserved in all eukaryotes (Supplementary Figure S15b).

Mdc1 forms a super-scaffold after DNA damage

From a macroscopic viewpoint, a major effect of Mdc1 Thr-4 phosphorylation is to stabilize formation of a approximately 4000 residue dimeric 'super-scaffold' containing two FHA domains and two BRCT-repeat modules. Although the major means by which broken DNA ends are maintained in proximity for efficient repair is through the bridging function of the MRN complex (49), it may be that Mdc1 dimers play a contributing role in stabilizing more global structure within chromatin loops containing damage sites (50–52) (Figure 7a, left). Such a 'velcro' model may also participate in an overall modulation of local chromatin compaction. Moreover, the existence of two BRCT-repeat domains within the Mdc1 dimer, and the significant effects of Mdc1 loss on fertility and spermatogenesis (9) may be indicative of a bridging role in meiotic crossover events. More recently, a model has been proposed in which Mdc1 self-association permits multiple C-terminal BRCT-repeat interactions that, simultaneously, tether Mdc1 to damaged chromatin via interaction with γH2AX and recruit phosphorylated forms of the putative histone H4-K20 methyltransferase, MMSET (39) (Figure 7a, right). Although our data show only small effects of Mdc1 dimer disruption on 53BP1 recruitment, this mechanism may still be of relevance for Mdc1 coupling to other proposed BRCT domain interactors (53).

Dimerization as a direct regulator of Mdc1–FHA interactions

Mdc1 appears to be the major interacting partner of its own FHA domain and we have presented a substantial body of evidence that this self-interaction is mediated by head-to-tail binding of pThr-4 within the N-terminal region, with the canonical FHA domain phospho-binding site. Our proteomic data show that FHA domain interactions with at least a subset of putative cellular partners are both negatively (DCAF1/DDB1) and positively (RNF95) impacted by ATM-dependent dimerization. Although somewhat unexpected, these observations are entirely consistent with our structural and biochemical data (Figure 7b). Firstly, pThr-4-mediated dimerization would be expected to occlude the canonical FHA

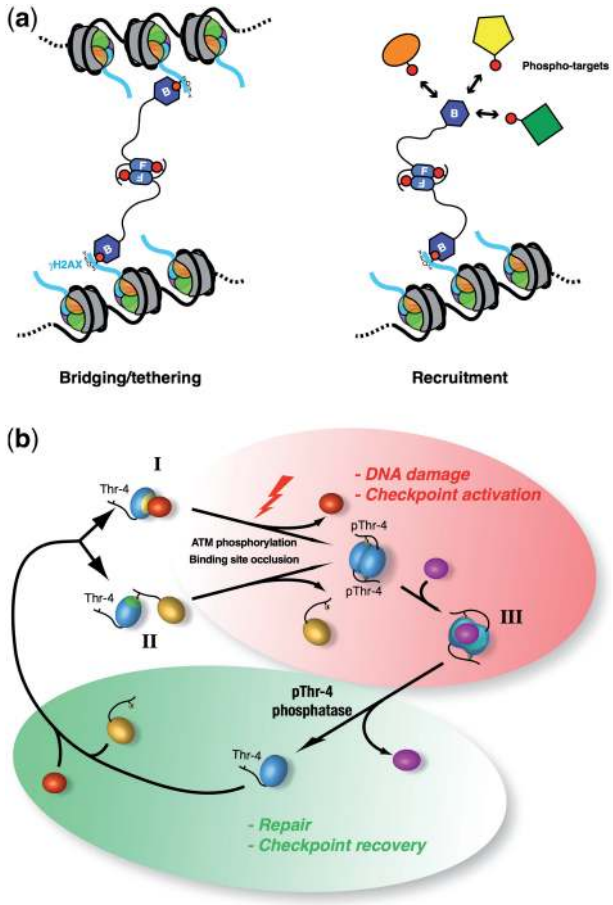

Figure 7. Dimerization regulates Mdc1 assembly and FHA domain interactions. (**a**) Dimeric Mdc1 as a super-scaffold. (Left) BRCT-repeat domains within the dimer can interact with γH2AX fulfilling a potential tethering function. (Right) Localization of Mdc1 dimers to damaged chromatin can occur through the canonical γH2AX interaction, leaving a free BRCT repeat domain to interact with other phosphorylated partners in the manner suggested for MMSET recruitment (39). (**b**) A regulatory cycle during DNA damage and repair—Binding of Thr-phosphorylated partners (gold) can occur through the canonical phospho-dependent surface (green patch) on the Mdc1–FHA (Mode I). Similarly, binding of phospho-independent partners (red) can occur through some or all of the Mdc1 dimerization interface (yellow) (Mode II). Following ATM-dependent Thr-4 phosphorylation and tight head-to-tail dimerization after DNA damage, both surfaces are occluded and their respective 'cargos' are released. Dimerization generates a new extended surface (cyan) (Mode III) for interaction with other factors (magenta) and this persists until the Mdc1–FHA dimer is disrupted by Thr-4 dephosphorylation.

domain phospho-binding surface (Type I) and/or the FHA–FHA interfacial region that could function as a phospho-independent binding surface prior to Thr-4 phosphorylation (Type II) and which acts in just this way in other FHA signaling systems (29): either mechanism could account for the interaction behavior of DCAF1/DDB1. Secondly, we surmise that Mdc1 dimerization might create new composite phospho-independent interaction surfaces spanning both FHA domains (Type III) and our SILAC analysis comparing binding ratios of wild-type and T4A mutant FHA domains suggest that binding to RNF95 might be regulated in this way. Indeed, an extensive, negatively charged surface spanning both FHA domains is evident in our crystal structures (Supplementary Figure S16). Thus, our data suggest a FHA interaction cycle that is potentially able to monitor and respond to each stage of the DDR, recruiting and/or releasing accessory repair and signaling factors in response to ATM and phosphatase activity.

CONCLUDING REMARKS

The fundamental importance of post-translational modifications, particularly serine/threonine phosphorylation, in DNA damage-dependent checkpoint establishment and the assembly of repair and signaling complexes is well established and Mdc1 has emerged as a focal point for many of these processes. Our data now reveal an unsuspected mode of Mdc1 regulation through ATM-dependent dimerization through its FHA domain and show how this phenomenon contributes to Mdc1 function through the damage repair cycle. Overall, our observations consolidate and extend the emerging significance of mediator self-association and provide the first insights into how this occurs at the structural level. In more general terms, our data reveal mechanisms for both positive and negative regulation of FHA domain interactions with phosphorylated and/or non-phosphorylated partners that will inform future studies of the myriad signaling pathways beyond the DDR that employ these versatile interaction modules.

ACCESSION NUMBERS

Coordinates and structure factors for the free and complexed Mdc1–FHA domains structures have been deposited with the Protein Data Bank under accession codes 3UN0 and 3UOT, respectively.

SUPPLEMENTARY DATA

Supplementary Data are available at NAR Online: Supplementary Methods, Supplementary Figures 1–16.

ACKNOWLEDGEMENTS

We thank Graeme Smith, Junje Chen and Steve Jackson for providing valuable reagents, Ian Taylor for assistance with MALLS, Katrin Rittinger for advice and assistance with ITC measurements and Philip Walker for help with X-ray data collection. S.J.S. would like to thank the Medical Research Council, UK (U117584228).

FUNDING

Novo Nordisk Foundation Center for Protein Research (to M.L.N.); European Commission's 7th Framework Programme grants Research Infrastructure Maximizing knowledge EXchange and access (XS) (INFRASTRUCTURES-F7-2010-262067/PRIME-XS) (to M.L.N.); Danish Cancer Society (to J.L. and C.L.); Danish National Research Foundation (to J.L. and

C.L.); Danish Medical research Council (to J.L. and C.L.); Swiss National Foundation (Grant Nr. 3100A0-111818 and 31003A-127450) (to M.S.); UBS AG (Im Auftrag eines Kunden) and the Kanton of Zürich (to M.S.); Medical Research Council, UK (U117584228) (to S.J.S.). Funding for open access charge: MRC, UK core.

Conflict of interest statement. None declared.

REFERENCES

1. Riches,L., Lynch,A. and Gooderham,N. (2008) Early events in the mammalian response to DNA double-strand breaks. *Mutagenesis*, **23**, 331–339.
2. Mohammad,D.H. and Yaffe,M.B. (2009) 14-3-3 proteins, FHA domains and BRCT domains in the DNA damage response. *DNA Repair*, **8**, 1009–1017.
3. Lou,Z., Minter-Dykhouse,K., Wu,X. and Chen,J. (2003) MDC1 is coupled to activated CHK2 in mammalian DNA damage response pathways. *Nature*, **421**, 957–961.
4. Stewart,G.S., Wang,B., Bignell,C.R., Taylor,A.M.R. and Elledge,S.J. (2003) MDC1 is a mediator of the mammalian DNA damage checkpoint. *Nature*, **421**, 961–966.
5. Goldberg,M., Stucki,M., Falck,J., D'Amours,D., Rahman,D., Pappin,D., Bartek,J. and Jackson,S.P. (2003) MDC1 is required for the intra-S-phase DNA damage checkpoint. *Nature*, **421**, 952–956.
6. Shang,Y.L., Bodero,A.J. and Chen,P.-L. (2003) NFBD1, a novel nuclear protein with signature motifs of FHA and BRCT, and an internal 41-amino acid repeat sequence, is an early participant in DNA damage response. *J. Biol. Chem.*, **278**, 6323–6329.
7. Jungmichel,S. and Stucki,M. (2010) MDC1: The art of keeping things in focus. *Chromosoma*, **119**, 337–349.
8. Stucki,M., Clapperton,J.A., Mohammad,D., Yaffe,M.B., Smerdon,S.J. and Jackson,S.P. (2005) MDC1 directly binds phosphorylated histone H2AX to regulate cellular responses to DNA double-strand breaks. *Cell*, **123**, 1213–1226.
9. Lou,Z., Minter-Dykhouse,K., Franco,S., Gostissa,M., Rivera,M.A., Celeste,A., Manis,J.P., van Deursen,J., Nussenzweig,A., Paull,T.T. *et al.* (2006) MDC1 maintains genomic stability by participating in the amplification of ATM-dependent DNA damage signals. *Mol. Cell*, **21**, 187–200.
10. So,S., Davis,A.J. and Chen,D.J. (2009) Autophosphorylation at serine 1981 stabilizes ATM at DNA damage sites. *J. Cell Biol.*, **187**, 977–990.
11. Xu,X. and Stern,D.F. (2003) NFBD1/MDC1 regulates ionizing radiation-induced focus formation by DNA checkpoint signaling and repair factors. *FASEB J.*, **17**, 1842–1848.
12. Zhang,J., Ma,Z., Treszezamsky,A. and Powell,S.N. (2005) MDC1 interacts with Rad51 and facilitates homologous recombination. *Nat. Struct. Mol. Biol.*, **12**, 902–909.
13. Spycher,C., Miller,E.S., Townsend,K., Pavic,L., Morrice,N.A., Janscak,P., Stewart,G.S. and Stucki,M. (2008) Constitutive phosphorylation of MDC1 physically links the MRE11-RAD50-NBS1 complex to damaged chromatin. *J. Cell Biol.*, **181**, 227–240.
14. Terwilliger,T. (2004) SOLVE and RESOLVE: automated structure solution, density modification and model building. *J.Synchrotron Radiat.*, **11**, 49–52.
15. McCoy,A.J. (2007) Solving structures of protein complexes by molecular replacement with Phaser. *Acta. Crystallogr. D. Biol. Crystallogr.*, **63**, 32–41.
16. Emsley,P. and Cowtan,K. (2004) Coot: model-building tools for molecular graphics. *Acta. Crystallogr. D. Biol. Crystallogr.*, **60**, 2126–2132.
17. Murshudov,G.N., Vagin,A.A. and Dodson,E.J. (1997) Refinement of macromolecular structures by the maximum-likelihood method. *Acta. Crystallogr. D. Biol. Crystallogr.*, **53**, 240–255.
18. Ong,S.-E., Blagoev,B., Kratchmarova,I., Kristensen,D.B., Steen,H., Pandey,A. and Mann,M. (2002) Stable isotope labeling by amino acids in cell culture, SILAC, as a simple and accurate approach to expression proteomics. *Mol. Cell Proteomics*, **1**, 376–386.
19. Olsen,J.V., Schwartz,J.C., Griep-Raming,J., Nielsen,M.L., Damoc,E., Denisov,E., Lange,O., Remes,P., Taylor,D., Splendore,M. *et al.* (2009) A dual pressure linear ion trap Orbitrap instrument with very high sequencing speed. *Mol. Cell Proteomics*, **8**, 2759–2769.
20. Hickson,I., Zhao,Y., Richardson,C.J., Green,S.J., Martin,N.M.B., Orr,A.I., Reaper,P.M., Jackson,S.P., Curtin,N.J. and Smith,G.C.M. (2004) Identification and characterization of a novel and specific inhibitor of the ataxia-telangiectasia mutated kinase ATM. *Cancer Res.*, **64**, 9152–9159.
21. Kolas,N.K., Chapman,J.R., Nakada,S., Ylanko,J., Chahwan,R., Sweeney,F.D., Panier,S., Mendez,M., Wildenhain,J., Thomson,T.M. *et al.* (2007) Orchestration of the DNA-damage response by the RNF8 ubiquitin ligase. *Science*, **318**, 1637–1640.
22. Mailand,N., Bekker-Jensen,S., Faustrup,H., Melander,F., Bartek,J., Lukas,C. and Lukas,J. (2007) RNF8 Ubiquitylates histones at DNA double-strand breaks and promotes assembly of repair proteins. *Cell*, **131**, 887–900.
23. Huen,M.S.Y., Grant,R., Manke,I., Minn,K., Yu,X., Yaffe,M.B. and Chen,J. (2007) RNF8 transduces the DNA-damage signal via histone ubiquitylation and checkpoint protein assembly. *Cell*, **131**, 901–914.
24. Durocher,D., Taylor,I.A., Sarbassova,D., Haire,L.F., Westcott,S.L., Jackson,S.P., Smerdon,S.J. and Yaffe,M.B. (2000) The molecular basis of FHA domain:phosphopeptide binding specificity and implications for phospho-dependent signaling mechanisms. *Mol. Cell*, **6**, 1169–1182.
25. Olsen,J.V., Vermeulen,M., Santamaria,A., Kumar,C., Miller,M.L., Jensen,L.J., Gnad,F., Cox,J., Jensen,T.S., Nigg,E.A. *et al.* (2010) Quantitative phosphoproteomics reveals widespread full phosphorylation site occupancy during mitosis. *Sci. Signal.*, **3**, ra3.
26. Luo,K., Yuan,J. and Lou,Z. (2011) Oligomerization of MDC1 protein is important for proper DNA damage response. *J. Biol. Chem.*, **286**, 28192–28199.
27. Li,J., Williams,B.L., Haire,L.F., Goldberg,M., Wilker,E., Durocher,D., Yaffe,M.B., Jackson,S.P. and Smerdon,S.J. (2002) Structural and functional versatility of the FHA domain in DNA-damage signaling by the tumor suppressor kinase Chk2. *Mol. Cell*, **9**, 1045–1054.
28. Mahajan,A., Yuan,C., Lee,H., Chen,E.S.-W., Wu,P.-Y. and Tsai,M.-D. (2008) Structure and function of the phosphothreonine-specific FHA domain. *Sci. Signal.*, **1**, re12.
29. Nott,T.J., Kelly,G., Stach,L., Li,J., Westcott,S., Patel,D., Hunt,D.M., Howell,S., Buxton,R.S., O'Hare,H.M. *et al.* (2009) An intramolecular switch regulates phosphoindependent FHA domain interactions in Mycobacterium tuberculosis. *Sci. Signal.*, **2**, ra12.
30. Li,J., Taylor,I.A., Lloyd,J., Clapperton,J.A., Howell,S., Macmillan,D. and Smerdon,S.J. (2008) Chk2 Oligomerization Studied by Phosphopeptide Ligation: IMPLICATIONS FOR REGULATION AND PHOSPHODEPENDENT INTERACTIONS. *J. Biol. Chem.*, **283**, 36019–36030.
31. Rodriguez,A. and Flemington,E.K. (1999) Transfection-mediated cell-cycle signaling: considerations for transient transfection-based cell-cycle studies. *Anal. Biochem.*, **272**, 171–181.
32. Melander,F., Bekker-Jensen,S., Falck,J., Bartek,J., Mailand,N. and Lukas,J. (2008) Phosphorylation of SDT repeats in the MDC1 N terminus triggers retention of NBS1 at the DNA damage-modified chromatin. *J. Cell Biol.*, **181**, 213–226.
33. Chapman,J.R. and Jackson,S.P. (2008) Phospho-dependent interactions between NBS1 and MDC1 mediate chromatin retention of the MRN complex at sites of DNA damage. *EMBO Rep.*, **9**, 795–801.
34. Wu,L., Luo,K., Lou,Z. and Chen,J. (2008) MDC1 regulates intra-S-phase checkpoint by targeting NBS1 to DNA double-strand breaks. *Proc. Natl. Acad. Sci. USA*, **105**, 11200–11205.
35. Lukas,C., Falck,J., Bartkova,J., Bartek,J. and Lukas,J. (2003) Distinct spatiotemporal dynamics of mammalian checkpoint regulators induced by DNA damage. *Nat. Cell Biol.*, **5**, 255–260.

36. Lukas,C., Melander,F., Stucki,M., Falck,J., Bekker-Jensen,S., Goldberg,M., Lerenthal,Y., Jackson,S.P., Bartek,J. and Lukas,J. (2004) Mdc1 couples DNA double-strand break recognition by Nbs1 with its H2AX-dependent chromatin retention. *EMBO J.*, **23**, 2674–2683.
37. Dimitrova,N. and de Lange,T. (2006) MDC1 accelerates nonhomologous end-joining of dysfunctional telomeres. *Genes Dev.*, **20**, 3238–3243.
38. Xu,X., Tsvetkov,L.M. and Stern,D.F. (2002) Chk2 activation and phosphorylation-dependent oligomerization. *Mol. Cell Biol.*, **22**, 4419–4432.
39. Pei,H., Zhang,L., Luo,K., Qin,Y., Chesi,M., Fei,F., Bergsagel,P.L., Wang,L., You,Z. and Lou,Z. (2011) MMSET regulates histone H4K20 methylation and 53BP1 accumulation at DNA damage sites. *Nature*, **470**, 124–128.
40. Soulier,J. and Lowndes,N.F. (1999) The BRCT domain of the S. cerevisiae checkpoint protein Rad9 mediates a Rad9-Rad9 interaction after DNA damage. *Curr. Biol.*, **9**, 551–554.
41. Usui,T., Foster,S.S. and Petrini,J.H.J. (2009) Maintenance of the DNA-damage checkpoint requires DNA-damage-induced mediator protein oligomerization. *Mol. Cell*, **33**, 147–159.
42. Kilkenny,M.L., Doré,A.S., Roe,S.M., Nestoras,K., Ho,J.C.Y., Watts,F.Z. and Pearl,L.H. (2008) Structural and functional analysis of the Crb2-BRCT2 domain reveals distinct roles in checkpoint signaling and DNA damage repair. *Genes Dev.*, **22**, 2034–2047.
43. Adams,M.M., Wang,B., Xia,Z., Morales,J.C., Lu,X., Donehower,L.A., Bochar,D.A., Elledge,S.J. and Carpenter,P.B. (2005) 53BP1 oligomerization is independent of its methylation by PRMT1. *Cell Cycle*, **4**, 1854–1861.
44. Ward,I., Kim,J.-E., Minn,K., Chini,C.C., Mer,G. and Chen,J. (2006) The tandem BRCT domain of 53BP1 is not required for its repair function. *J. Biol. Chem.*, **281**, 38472–38477.
45. Zgheib,O., Pataky,K., Brugger,J. and Halazonetis,T.D. (2009) An oligomerized 53BP1 tudor domain suffices for recognition of DNA double-strand breaks. *Mol. Cell Biol.*, **29**, 1050–1058.
46. Lee,G.-I., Ding,Z., Walker,J.C. and Van Doren,S.R. (2003) NMR structure of the forkhead-associated domain from the Arabidopsis receptor kinase-associated protein phosphatase. *Proc. Natl. Acad. Sci. USA*, **100**, 11261–11266.
47. Ahn,J. and Prives,C. (2002) Checkpoint kinase 2 (Chk2) monomers or dimers phosphorylate Cdc25C after DNA damage regardless of threonine 68 phosphorylation. *J. Biol. Chem.*, **277**, 48418–48426.
48. Cai,Z., Chehab,N.H. and Pavletich,N.P. (2009) Structure and activation mechanism of the CHK2 DNA damage checkpoint kinase. *Mol. Cell*, **35**, 818–829.
49. Williams,R.S., Moncalian,G., Williams,J.S., Yamada,Y., Limbo,O., Shin,D.S., Groocock,L.M., Cahill,D., Hitomi,C., Guenther,G. *et al.* (2008) Mre11 dimers coordinate DNA end bridging and nuclease processing in double-strand-break repair. *Cell*, **135**, 97–109.
50. Bassing,C.H. and Alt,F.W. (2004) H2AX may function as an anchor to hold broken chromosomal DNA ends in close proximity. *Cell Cycle*, **3**, 149–153.
51. Franco,S., Gostissa,M., Zha,S., Lombard,D.B., Murphy,M.M., Zarrin,A.A., Yan,C., Tepsuporn,S., Morales,J.C., Adams,M.M. *et al.* (2006) H2AX prevents DNA breaks from progressing to chromosome breaks and translocations. *Mol. Cell*, **21**, 201–214.
52. van Gent,D.C. and van der Burg,M. (2007) Non-homologous end-joining, a sticky affair. *Oncogene*, **26**, 7731–7740.
53. Coster,G. and Goldberg,M. (2010) The cellular response to DNA damage: A focus on MDC1 and its interacting proteins. *Nucleus*, **1**, 166–178.